Am J Nucl Med Mol Imaging 2023;13(1):18-25
www.ajnmmi.us /ISSN:2160-8407/ajnmmi0147353

Original Article

Assessment of the correlation between arterial lumen density and its metabolic activity in atherosclerotic patients using ^{18}F-FDG positron emission tomography/computed tomography

Mamdouh S Al-Enezi

Department of Diagnostic Radiology, College of Applied Medical Sciences, University of Hail, Hail, Saudi Arabia

Received October 29, 2022; Accepted January 20, 2023; Epub February 15, 2023; Published February 28, 2023

Abstract: Large lipid core (extended into arterial lumen) and high density of macrophages (associated with ^{18}F-fluorodeoxyglucose "^{18}F-FDG" uptake) in atherosclerotic plaque were shown to be an overt feature of plaque rupture. Nineteen participants were imaged with computed tomography (CT) and positron emission tomography (PET) with ^{18}F-FDG in a dynamic mode. The mean lumen density in Hounsfield unit (HU) was measured per region of interest (ROI) on CT images and classified as non-calcified and calcified classifications. Calcified group was divided into partially calcified and calcified groups. Metabolic rate of glucose (MRG) was computed per ROI on PET dynamic images using modified 2-tissue compartmental model that is independent of partial volume effect. Data is clustered using Automatic Hierarchical K-means algorithm (AKH) with silhouette-coefficient. Arterial segments of 1180 ROIs for Aorta and iliac arteries were classified as non-calcified and calcified segments and clustered using AHK with respect to the mean of intravascular attenuation (in HU). There was a statistical difference in MRG corresponded to low intravascular attenuation cluster compared to higher intravascular attenuation clusters ($P<0.05$), but not within higher clusters ($P>0.05$), for both non-calcified and calcified classes. In partially calcified segments, same pattern was observed as the low intravascular attenuation cluster was accompanied with significant metabolic activity but not for calcified segments. Low intravascular attenuation is associated with high MRG measured on ^{18}F-FDG PET images, which may reflect the instability of atherosclerotic plaque. Partially calcified plaque is metabolically active compared to calcified plaque.

Keywords: Atherosclerosis, lumen density, metabolic activity, ^{18}F-FDG, PET, CT

Introduction

Atherosclerosis is the main complication factor for cardiovascular disease and stroke, and the leading cause of mortality and morbidity worldwide. It is started through the buildup of atherosclerotic plaque within the vessel wall. Atherosclerotic plaque is composed of fatty substances, inflammatory cells, and matrix elements in addition to calcification [1]. Atherosclerotic plaque goes through initiation stage, progression stage and vulnerable stage, this stage depicts the highest severity and causes acute clinical complication of atherosclerosis including disability and sudden death. Therefore, vulnerable plaque is now known to be characterized by large lipid core encapsulated by thin fibrous cap [2]. Lumenographic imaging techniques and particularly digital subtraction angiography provide an excellent spatial resolution for the detection of plaque stenosis; however, stenosis is not per se a representative of vulnerable plaque but the inflammation represented by the accumulation of activated macrophages [3, 4]. Another imaging modality used in atherosclerosis settings is intravascular ultrasound, in addition to its invasive nature, intrinsic and extrinsic artifacts may interfere with image interpretation [5]. Computed tomography (CT) scan is plentifully used in atherosclerosis for calcification burden in the utilization of Agatston method or other calcification score methods. It has been recently demonstrated that the lumen density in large plaque would decreased rapidly

[6, 7]. Additionally, plaque burden has been adjusted as a function of lumen density in some studies [8]. Molecular imaging with positron emission tomography/computed tomography (PET/CT) has the ability in detecting different stages of atherosclerotic plaque in addition to different progression phases [9], thus, PET/CT could accurately identify the vulnerable plaque. ^{18}F-fluorodeoxyglucose (^{18}F-FDG) is a glucose analog tracer that is directly proportional to the density of macrophages within the plaque [9]. Density of macrophages is a potential biomarker of vulnerable plaque [10].

A major challenge of ^{18}F-FDG-PET/CT is the quantification of ^{18}F-FDG uptake in the setting of atherosclerosis. Pharmacokinetic features of dynamic ^{18}F-FDG-PET/CT are more accurately reflect the metabolic rate of ^{18}F-FDG in comparison to other semi-quantitative measurements. Other challenge that has not to be overlooked in atherosclerosis imaging and quantification protocols due to small area of arterial walls is partial volume effect. We have recently proposed a mathematical modeling of pharmacokinetics independent of partial volume effect [11].

Data of oncological patients is utilized in a tremendous analytical studies in the regard of atherosclerosis, where the influence of anticancer medical therapies in tracer uptake cannot be excluded, as a result, the accuracy and reproducibility of the analysis is questionable [12]. The aim of this work is to see whether a lumen density could reveal a correlation with metabolic rate of ^{18}F-FDG in cross sectional analysis for atherosclerotic (non-oncological) patients.

Materials and methods

Current retrospective study has been approved by the research ethics committee of the Faculty of Medicine and Health Sciences, University of Sherbrooke, Canada.

All participants gave a written informed consent for scanning with ^{18}F-FDG-PET/CT.

Study design

The dynamic PET data were acquired in 10 seconds per time frame continuously from 0 to 2-min, in 30 seconds per time frame continuously from 2-min to 6-min and in 4 min per time frame continuously from 6-min to 30-min. The acquired data were obtained of 19 participants (69.2 ± 3.65 years old). The images were acquired on Philips Gemini TF 16 scanner immediately after ^{18}F-FDG bolus injection of 140 to 400 MBq that is normalized to participant's weight and the data were reconstructed into 26 frames using 3D row action maximum likelihood reconstruction algorithm in an image array of 144×144×45 voxels with a voxel size of 1×1×4 mm^3 and data were attenuation corrected using CT images. Participants have undergone an overnight fasting period of at least 8 hours prior to ^{18}F-FDG PET/CT scans. Glycemia was measured at the beginning of the protocol for each participant, and the average glycemia was 5.00 ± 0.70 mmol/l (mean ± standard deviation "STD") with maximum and minimum glycemia of 6.10 and 3.90 mmol/l that is well below 7.00 mmol/l, based on the guidelines of atherosclerosis imaging with ^{18}F-FDG PET [13].

PET image segmentation was performed on the first 2 minutes and a region of interest (ROI) was constructed as a binary image automatically using edge-based active contours algorithm [14]. Arteries on CT images were first identified per slice, and the arterial boundary is determined using edge-based active contours algorithm as in PET image. The calcification was computed as areas greater than 2 contiguous pixels with intensity greater than 130 Hounsfield units (HU) on the segmented artery [15].

Metabolic rate of glucose (MRG) on dynamic PET image was computed per ROI using a modified 2-tissue compartmental model that is independent of partial volume effect and it is explained in detail elsewhere [11].

The ROI of lumen was made by prior knowledge of arterial diameter, where the lumen diameter is computed as $\frac{2r}{3}$ (mm) [16] and constructed using lumen diameter obtained from the previous equation with respect to the center of gravity of arterial ROI using MATLAB R2016b. The mean lumen density (in HU) was measured per ROI and clustered using Automatic Hierarchical K-means algorithm (AHK) [17] and its performance was enhanced by applying silhouette-coefficient [18]. The mean lumen density of all segments was divided into two groups: non-

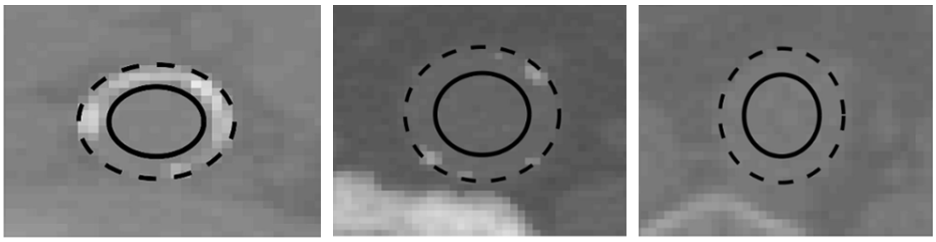

Lumen attenuation:	48.60 ± 18.63 HU	45.43 ± 20.20 HU	45.44 ± 17.48 HU
Lumen area:	168.33 mm^2	259.50 mm^2	195.25 mm^2
Average lumen diameter:	14.80 mm	18.46 mm	15.77 mm

Figure 1. Representative cross-sectional images showing three types of arterial segments, calcified, partially calcified and non-calcified. The contours of the arteries indicated by dotted ROIs were delineated automatically using edge-based active contours (fitted with circle shape) and solid line on the center of the cross-sectional for the measurement of luminal attenuation values.

Table 1. Summary of the attenuation values of clustered groups for non-calcified segments measured on CT images and metabolic rate of glucose (MRG) obtained from modified 2-tissue compartmental model

Cluster	MEASURES	ATTENUATION (HU)	MRG (μmole/100 g/min)
Group-1	Mean ± STD	23.98 ± 7.43	1.20 ± 0.66
	Median	26.05	1.09
	Quartiles	(29.38-20.99)	(1.54-0.69)
	IQR	8.39	0.85
Group-2	Mean ± STD	38.84 ± 3.99	1.01 ± 0.60
	Median	38.82	0.93
	Quartiles	(42.10-35.45)	(1.40-0.52)
	IQR	6.65	0.88
Group-3	Mean ± STD	52.54 ± 5.96	1.00 ± 0.58
	Median	51.00	0.95
	Quartiles	(55.20-48.27)	(1.30-0.47)
	IQR	6.93	0.85

calcified and calcified groups. The calcified group was further divided into 2 groups as calcified and partially calcified (spotty of calcification) groups.

Statistical analysis

Continuous data were tested for normality in the utilization of D'Agostino-Pearson omnibus test. Continuous variables were expressed in mean ± STD for normally distributed data and in median with interquartile range (IQR) for skewed distributions. Statistical significance was assumed for *P*-values <0.05.

Results

A total of 1180 segments of Aorta in addition to left and right iliac arteries were included in the analysis for PET and CT images of 19 participants averaging about 62 segments per participant. Total attenuation value was 39.90 HU ± 9.91 (mean ± STD), 40.26 HU, 11.68 (median and IQR). There were 950 non-calcified segments, and 230 segments were with calcification. The overview of the lumen attenuation analysis is shown in **Figure 1**. If a slice included a large diffused calcified area, it was excluded, especially in bifurcation regions.

The mean attenuation of the lumen in non-calcified segments that were automatically clustered using AKH algorithm with silhouette-coefficient is shown in **Table 1**. While the data of calcified segments are summarized in **Table 2**.

In **Figure 2**, group-1 represents MRG values for lowest attenuation cluster, group-2 represents MRG values for midst attenuation cluster and group-3 represents MRG values for highest attenuation clusters.

By comparing the metabolic activity corresponded to the 3 clusters of lumen attenuation in non-calcified segments, there was a statistical difference in MRG measured on ^{18}F-FDG PET images between group-1 compared to both higher attenuation groups with *P*-values of 0.02 and 0.04 for group-2 and group-3 respectively. However, those groups (group-2 and group-3) when compared to each other, they did not show a statistical significance in metabolic

Table 2. Summary of the attenuation values of clustered groups for calcified segments measured on CT images and metabolic rate of glucose (MRG) obtained from modified 2-tissue compartmental model

Cluster	MEASURES	ATTENUATION (HU)	MRG (μmole/100 g/min)
Group-1	Mean ± STD	32.74 ± 7.91	1.35 ± 0.52
	Median	35.13	1.33
	Quartiles	(38.23-30.00)	(1.55-0.93)
	IQR	8.23	0.62
Group-2	Mean ± STD	48.11 ± 4.50	0.91 ± 0.63
	Median	38.82	0.82
	Quartiles	(51.40-44.35)	(1.21-0.46)
	IQR	7.05	0.74
Group-3	Mean ± STD	68.65 ± 9.90	0.70 ± 0.54
	Median	65.92	0.57
	Quartiles	(73.00-61.75)	(0.90-0.42)
	IQR	11.25	0.48

activity (*P*-value = 0.72). The results are shown in aka box and whisker plot in **Figure 2A**.

Similarly, calcified segments were evaluated in the same way. The same pattern was observed, where the lowest attenuation group (group-1) was statistically significantly greater in MRG compared to other higher groups with *P*-values of 0.004 and 0.001 for group-2 and group-3 respectively. Yet, those groups did not vary significantly among each other (*P*-value = 0.35). The results are depicted by aka box and whisker plot in **Figure 2B**.

When the calcified segments were distributed into two groups as partially calcified group and calcified group by histogram thresholding, and applying automatic AKH algorithm on each group and clustered into 3 clusters each, a statistical difference was observed in a cluster of lowest attenuation (group-1) compared to other higher clusters (group-2 and group-3) of partially calcified clusters, *P*-values with respect to group-1 where 0.02 and 0.03 for group-2 and group-3 respectively, and there was no statistical difference between group-2 and group-3 (*P*-value = 0.93). However, all three clusters in the calcified group were not statistically significant among each other (*P*-values >0.05).

Lastly, by comparing non-calcified, partially calcified, and calcified segments, group of non-calcified and group of partially calcified segments did not show a statistical significance among each other (*P*-values >0.05), while the group of calcified segments statistically significantly lower in terms of metabolic rate of activity compared to non-calcified and partially calcified segments (*P*-values <0.05). The mean HU was 51.53 ± 5.90 (median and IQR, 51, 6.92), 43.1 ± 3.20 (median and IQR, 42.05, 3.67) and 65.35 ± 10.80 (median and IQR, 62.22, 11.36) for the group of non-calcified, partially calcified, and calcified segments respectively, where both first two groups with respect to the first cluster class where statistically significantly different in attenuation compared with the later (*P*-values were 0.002 and 0.001 for non-calcified and partially calcified segments respectively), but they did not statistically vary among each other (*P*-value = 0.58).

Discussion

The presented approach seemingly the first attempt to investigate the possibility of correlating lumen attenuation measured on CT images with metabolic activity measured on ^{18}F-FDG PET images that has a potential in examining different biological markers of the plaque.

^{18}F-FDG is the best-studied, validated, and routinely used PET tracer for atherosclerosis imaging. Nevertheless, other Functional PET imaging radiotracers have been utilized in targeting molecular elements of atherosclerosis. ^{18}F-NaF is a tracer targeting the formation of microcalcification [19], the presence of microcalcification is thought to identify vulnerable plaques [20, 21], thus it gives new insight of atherosclerosis as an alternative approach to the glucose metabolism in monitoring and assessing the atherosclerosis disease state [22]. DOTATATE ([1,4,7,10-tetraazacyclododecane-N,N',N'',N'''-tetraacetic acid]-d-Phe1,Tyr3-octrotate) is another radiopharmaceutical utilized for atherosclerosis and good correlation between its uptake with calcification burden and cardiovascular risk factors, such as age and hypertension, had been demonstrated [23]. Yet, it is comparable with ^{18}F-FDG [24]. Recently, CXCR4-^{68}Ga-Pentixafor tracer has been shown to identify

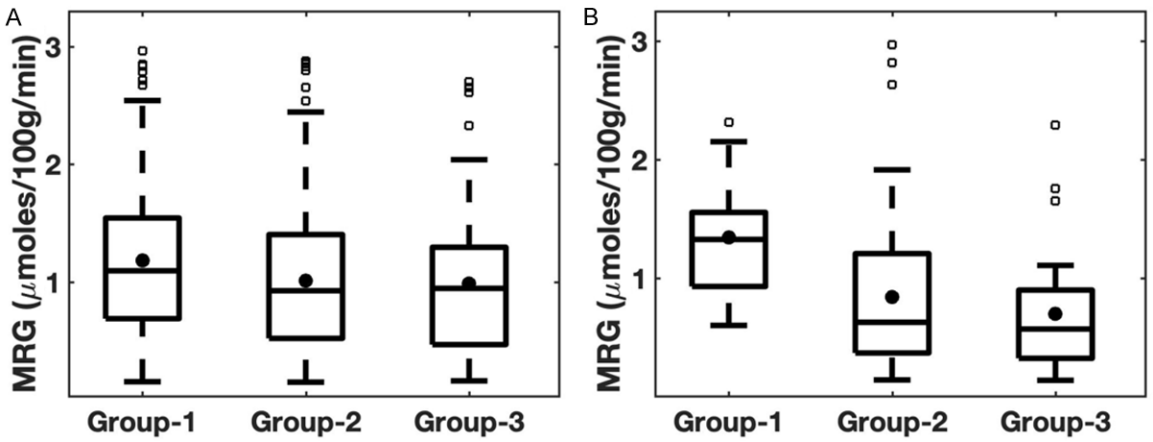

Figure 2. Box and whisker plot shows the relations of metabolic activity corresponded to 3 groups of clusters for lumen attenuation in non-calcified segments (A) and the same for calcified segments in (B). Group-1 represents MRG values for lowest attenuation cluster, group-2 represents MRG values for midst attenuation cluster and group-3 represents MRG values for highest attenuation clusters.

atherosclerosis in early stage. However, the complexity of the dynamics of CXCR4 expression in atherosclerosis and its specificity making the meaning of its uptake more challenging compared to ^{18}F-FDG [25].

Because of the limited spatial resolution of CT scanner which hinder the ability to classify atherosclerotic plaque that is not calcified as a function of its morphologic features rather than the presence of calcification, thus, most studies in this domain classified non-calcified plaque into two categories, low X-ray attenuation atherosclerotic plaque to reflect lipid-rich plaque and high X-ray attenuation atherosclerotic plaque to reflect fibroatheromas plaque, within a specified attenuation window to avoid the effect of attenuation overlapping. Such a way shows good accuracy with a correlation coefficient of 81% to 83% and 94% for lipid-rich plaque and fibroatheromas plaque respectively [26, 27]. However, the presence of hemorrhage and other factors could limit its reliability leading to float those two kinds into a single type named non-calcified plaque [28].

Lumen attenuation may give new insight into atherosclerotic plaque. Plaque attenuation has been shown to be significantly affected by lumen contrast in both ex-vivo and in-vivo [29]. Additionally, plaques of larger lipid cores that may incorporated into lumen attenuation was shown to be one of vulnerability markers by a study of 88 sudden cardiac death cases in addition to the presence of high density of macrophages in those cardiac death cases [30]. Moreover, high density of macrophages is strongly correlated with ^{18}F-FDG uptake [31]. Therefore, the lumen attenuation could be affected accordingly in the presence of large lipid core of the plaque. This may explain the statistical significance of low attenuation cluster as a function of MRG in non-calcified segments. Although a study of by M Kidoh et al. [32], indicated that the plaque attenuation on nonenhanced coronary artery images is independent of lumen attenuation, however, the misregistration from enhanced into nonenhanced CT images and motion could apparently affect the accurate placement of ROI and therefore the analysis. Such an issue that may lead to a reduction in the accuracy has been demonstrated by them in their recently published work for a phantom study [33].

Interestingly, in addition to non-calcified plaque, partially calcified (spotty of calcification) plaque has been demonstrated in several studies to be a marker of high-risk morphology plaque that causes the instability of atherosclerotic plaque due to several factors including the sheer stress and may lead to plaque rupture. This is in the agreement with the findings of the presented work, where the partially calcified but not calcified segments were statistically correlated with high MRG [34-37].

Although, this initial study was performed on non-oncological patients, as a result, the effect of anticancer medical therapies on ^{18}F-FDG

uptake [12] is unlikely, which increases the accuracy of metabolic activity measurements in this study. However, the method has some limitations. First, CT digital subtraction angiography is more accurate in identifying the arterial lumen, and if avoiding misregistration, the outcomes would be more precise to highlight the feasibility of the current methodology. Second, the presented results may be dependent upon the CT unit used, reconstruction algorithm, adaptive filter (kernel), pixel size, slice thickness, and other scanning parameters. Lastly, a limited number of participants that have been included in this initial exploratory study. Additional large-scale prospective studies are needed to confirm the observations in this initial study.

Conclusion

The low intravascular attenuation computed on CT scan is accompanied with high metabolic activity measured on ^{18}F-FDG PET scan, which may reflect the instability of atherosclerotic plaque. Therefore, large lipid rich plaque that is non-calcified could be identified on CT images with intravascular attenuation that was shown to be statistically correlated with the density of macrophages represented by ^{18}F-FDG uptake. Partially calcified plaque is metabolically active compared to calcified plaque.

Acknowledgements

The author wishes to thank Dr. M Bentourkia, Dr. Éric Turcotte, Éric Lavallee and the clinical team at the Sherbrooke Molecular Imaging Centre, Université de Sherbrooke, for their technical assistance.

Disclosure of conflict of interest

None.

Address correspondence to: Dr. Mamdouh S Al-Enezi, Department of Diagnostic Radiology, College of Applied Medical Sciences, University of Hail, PO Box 2440, Hail 81451, Saudi Arabia. Tel: +966-553-344-1195; Fax: +966165310168; E-mail: ms.alenezi@uoh.edu.sa

References

[1] Mehu M, Narasimhulu CA and Singla DK. Inflammatory cells in atherosclerosis. Antioxidants 2022; 11: 233.

[2] Fishbein MC. The vulnerable and unstable atherosclerotic plaque. Cardiovasc Pathol 2010; 19: 6-11.

[3] Mortensen MB, Dzaye O, Steffensen FH, Bøtker HE, Jensen JM, Rønnow Sand NP, Kragholm KH, Sørensen HT, Leipsic J, Mæng M, Blaha MJ and Nørgaard BL. Impact of plaque burden versus stenosis on ischemic events in patients with coronary atherosclerosis. J Am Coll Cardiol 2020; 76: 2803-2813.

[4] Van Der Toorn JE, Bos D, Ikram MK, Verwoert GC, Van Der Lugt A, Ikram MA, Vernooij MW and Kavousi M. Carotid plaque composition and prediction of incident atherosclerotic cardiovascular disease. Circ Cardiovasc Imaging 2022; 15: e013602.

[5] Anderson JD and Kramer CM. MRI of atherosclerosis: diagnosis and monitoring therapy. Expert Rev Cardiovasc Ther 2007; 5: 69-80.

[6] Pennell D, Delgado V, Knuuti J, Maurovich-Horvat P and Bax JJ. The year in cardiology: imaging the year in cardiology 2019. Eur Heart J 2020; 41: 739-747.

[7] Rodriguez-Granillo GA, Carrascosa PM and García MJ. Dual energy CT imaging for the assessment of coronary artery stenosis. Springer Cham 2015; 1: 173-193.

[8] Lerman JB, Joshi AA, Chaturvedi A, Aberra TM, Dey AK, Rodante JA, Salahuddin T, Chung JH, Rana A, Teague HL, Wu JJ, Playford MP, Lockshin BA, Chen MY, Sandfort V, Bluemke DA and Mehta NN. Coronary plaque characterization in psoriasis reveals high-risk features that improve after treatment in a prospective observational study. Circulation 2017; 136: 263-276.

[9] Bassir A, Raynor WY, Park PSU, Werner TJ, Alavi A and Revheim ME. Molecular imaging in atherosclerosis. Clin Trans Imaging 2022; 10: 259-272.

[10] Zhang M, Xie Z, Long H, Ren K, Hou L, Wang Y, Xu X, Lei W, Yang Z, Ahmed S, Zhang H and Zhao G. Current advances in the imaging of atherosclerotic vulnerable plaque using nanoparticles. Mater Today Bio 2022; 14: 100236.

[11] Al-Enezi MS and Bentourkia M. Kinetic modeling of dynamic PET-^{18}F-FDG atherosclerosis without blood sampling. IEEE Trans Radiat Plasma Med Sci 2020; 4: 729-734.

[12] Li X, Heber D, Cal-Gonzalez J, Karanikas G, Mayerhoefer ME, Rasul S, Beitzke D, Zhang X, Agis H, Mitterhauser M, Wadsak W, Beyer T, Loewe C and Hacker M. Association between osteogenesis and inflammation during the progression of calcified plaque evaluated by ^{18}F-fluoride and ^{18}F-FDG. J Nucl Med 2017; 58: 968-974.

[13] Bucerius J, Hyafil F, Verberne HJ, Slart RH, Lindner O, Sciagra R, Agostini D, Übleis C, Gimelli A and Hacker M; Cardiovascular Commit-

tee of the European Association of Nuclear Medicine (EANM). Position paper of the cardiovascular committee of the European Association of Nuclear Medicine (EANM) on PET imaging of atherosclerosis. Eur J Nucl Med Mol Imaging 2016; 43: 780-792.

[14] Caselles V, Kimmel R and Sapiro G. Geodesic active contours. Int J Comput Vis 1997; 22: 61-79.

[15] van der Bijl N, Joemai RM, Geleijns J, Bax JJ, Schuijf JD, de Roos A and Kroft LJ. Assessment of agatston coronary artery calcium score using contrast-enhanced CT coronary angiography. AJR Am J Roentgenol 2010; 195: 1299-1305.

[16] Saba L, Gao H, Raz E, Sree SV, Mannelli L, Tallapally N, Molinari F, Bassareo PP, Acharya UR, Poppert H and Suri JS. Semiautomated analysis of carotid artery wall thickness in MRI. J Magn Reson Imaging 2014; 39: 1457-1467.

[17] Filzmoser P, Baumgartner R and Moser E. A hierarchical clustering method for analyzing functional MR images. Magn Reson Imaging 1999; 17: 817-826.

[18] Rousseeuw PJ. Silhouettes: a graphical aid to the interpretation and validation of cluster analysis. J Comput Appl Math 1987; 20; 53-65.

[19] Aikawa E, Nahrendorf M, Figueiredo JL, Swirski FK, Shtatland T, Kohler RH, Jaffer FA, Aikawa M and Weissleder R. Osteogenesis associates with inflammation in early-stage atherosclerosis evaluated by molecular imaging in vivo. Circulation 2007; 116: 2841-2850.

[20] Derlin T, Richter U, Bannas P, Begemann P, Buchert R, Mester J and Klutmann S. Feasibility of 18F-sodium fluoride PET/CT for imaging of atherosclerotic plaque. J Nucl Med 2010; 51: 862-865.

[21] Joshi NV, Vesey AT, Williams MC, Shah AS, Calvert PA, Craighead FH, Yeoh SE, Wallace W, Salter D, Fletcher AM, van Beek EJ, Flapan AD, Uren NG, Behan MW, Cruden NL, Mills NL, Fox KA, Rudd JH, Dweck MR and Newby DE. 18F-fluoride positron emission tomography for identification of ruptured and high-risk coronary atherosclerotic plaques: a prospective clinical trial. Lancet 2014; 383: 705-713.

[22] Rojulpote C, Borja AJ, Zhang V, Aly M, Koa B, Seraj SM, Raynor WY, Kothekar E, Kaghazchi F, Werner TJ, Gerke O, Høilund-Carlsen PF and Alavi A. Role of 18F-NaF-PET in assessing aortic valve calcification with age. Am J Nucl Med Mol Imaging 2020; 10: 47-56.

[23] Li X, Samnick S, Lapa C, Israel I, Buck AK, Kreissl MC and Bauer W. 68Ga-DOTATATE PET/CT for the detection of inflammation of large arteries: correlation with ^{18}F-FDG, calcium burden and risk factors. EJNMMI Res 2012; 2: 52.

[24] Tarkin JM, Joshi FR, Evans NR, Chowdhury MM, Figg NL, Shah AV, Starks LT, Martin-Garrido A, Manavaki R, Yu E, Kuc RE, Grassi L, Kreuzhuber R, Kostadima MA, Frontini M, Kirkpatrick PJ, Coughlin PA, Gopalan D, Fryer TD, Buscombe JR, Groves AM, Ouwehand WH, Bennett MR, Warburton EA, Davenport AP and Rudd JH. Detection of atherosclerotic inflammation by ^{68}Ga-DOTATATE PET compared to ^{18}F-FDG PET imaging. J Am Coll Cardiol 2017; 69: 1774-1791.

[25] Kircher M, Tran-Gia J, Kemmer L, Zhang X, Schirbel A, Werner RA, Buck AK, Wester HJ, Hacker M, Lapa C and Li X. Imaging inflammation in atherosclerosis with CXCR4-directed 68Ga-pentixafor PET/CT: correlation with ^{18}F-FDG PET/CT. J Nucl Med 2020; 61: 751-756.

[26] Brodoefel H, Reimann A, Heuschmid M, Tsiflikas I, Kopp AF, Schroeder S, Claussen CD, Clouse ME and Burgstahler C. Characterization of coronary atherosclerosis by dual-source computed tomography and HU-based color mapping: a pilot study. Eur Radiol 2008; 18: 2466-2474.

[27] Shen Y, Qian JY, Wang MH, Liu Y, Liu XB, Ge L, Ma JY and Ge JB. Quantitative and qualitative assessment of non-obstructive left main coronary artery plaques using 64-multislice computed tomography compared with intravascular ultrasound. Chin Med J (Engl) 2010; 123: 827-833.

[28] Daghem M, Bing R, Fayad ZA and Dweck MR. Noninvasive imaging to assess atherosclerotic plaque composition and disease activity: coronary and carotid applications. JACC Cardiovasc Imaging 2020; 13: 1055-1068.

[29] Cademartiri F, Runza G, Palumbo A, Maffei E, Martini C, McFadden E, Somers P, Knaapen M, Verheye S, Weustink AC, Mollet NR, De Feyter PJ, Hamers R and Bruining N. Lumen enhancement influences absolute noncalcific plaque density on multislice computed tomography coronary angiography: ex-vivo validation and in-vivo demonstration. J Cardiovasc Med (Hagerstown) 2010; 11: 337-344.

[30] Varnava AM, Mills PG and Davies MJ. Relationship between coronary artery remodeling and plaque vulnerability. Circulation 2002; 105: 939-943.

[31] Mikail N, Meseguer E, Lavallée P, Klein I, Hobeanu C, Guidoux C, Cabrejo L, Lesèche G, Amarenco P and Hyafil F. Evaluation of non-stenotic carotid atherosclerotic plaques with combined FDG-PET imaging and CT angiography in patients with ischemic stroke of unknown origin. J Nucl Cardiol 2022; 29: 1329-1336.

[32] Kidoh M, Utsunomiya D, Oda S, Funama Y, Nakaura T, Yuki H, Hirata K, Namimoto T and Ya-

mashita Y. Evaluation of the effect of intracoronary attenuation on coronary plaque measurements using a dual-phase coronary CT angiography technique on a 320-row CT scanner-in vivo validation study. Acad Radiol 2016; 23: 315-320.

[33] Funama Y, Oda S, Kidoh M, Sakabe D and Nakaura T. Effect of image quality on myocardial extracellular volume quantification using cardiac computed tomography: a phantom study. Acta Radiol 2022; 63: 159-165.

[34] Singh P, Emami H, Subramanian S, Maurovich-Horvat P, Marincheva-Savcheva G, Medina HM, Abdelbaky A, Alon A, Shankar SS, Rudd JH, Fayad ZA, Hoffmann U and Tawakol A. Coronary plaque morphology and the anti-inflammatory impact of atorvastatin: a multicenter 18F-fluorodeoxyglucose positron emission tomographic/computed tomographic study. Circ Cardiovasc Imaging 2016; 9: e004195.

[35] Achenbach S, Fuchs F, Goncalves A, Kaiser-Albers C, Ali ZA, Bengel FM, Dimmeler S, Fayad ZA, Mebazaa A, Meder B, Narula J, Shah A, Sharma S, Voigt JU and Plein S. Non-invasive imaging as the cornerstone of cardiovascular precision medicine. Eur Heart J Cardiovasc Imaging 2022; 23: 465-475.

[36] Pergola V, Cabrelle G, Mattesi G, Cattarin S, Furlan A, Dellino CM, Continisio S, Montonati C, Giorgino A, Giraudo C, Leoni L, Bariani R, Barbiero G, Bauce B, Mele D, Perazzolo Marra M, De Conti G, Iliceto S and Motta R. Added value of CCTA-derived features to predict MACEs in stable patients undergoing coronary computed tomography. Diagnostics (Basel) 2022; 12: 1446.

[37] Al-Enezi MS, Abdo RA, Mokeddem MY, Slimani FAA, Khalil A, Fulop T, Turcotte E and Bentourkia M. Assessment of artery calcification in atherosclerosis with dynamic ^{18}F-FDG-PET/CT imaging in elderly subjects. Int J Cardiovasc Imaging 2019; 35: 947-954.